Computational Materials Science 246 (2025) 113442

Contents lists available at ScienceDirect

Computational Materials Science

journal homepage: www.elsevier.com/locate/commatsci

Full length article

Modelling the influence of moisture on the mechanical behaviour of crosslinked polyurethane adhesives

S.P. Josyula [a,*], M. Brede [b], O. Hesebeck [b], K. Koschek [b], W. Possart [c], A. Wulf [b], B. Zimmer [c], S. Diebels [a]

[a] Chair of Applied Mechanics, Saarland University, Saarbrücken, Germany
[b] Fraunhofer Institute for Manufacturing Technology and Advanced Materials, Wiener Straße 12, Bremen, Germany
[c] Chair for Adhesion and Interphases in Polymers, Saarland University, Saarbrücken, Germany

ARTICLE INFO

Keywords:
Coupled material model
Crosslinked polyurethane adhesive
Micromechanical network model
Moisture diffusion
Moisture-dependent parameters

ABSTRACT

Crosslinked polymers are typically viscoelastic in nature and show non-linear behaviour due to large deformation. The mechanical behaviour of these polymers is influenced by moisture diffusion because of the hygroscopic properties of the material. The crosslinked polymers are formed by the shorter and longer chain length distribution. The shorter chains tend to break/debond from the network with an increase in the deformation thus leading to the softening of the material. In this paper, the crosslinked polymer mechanical behaviour is modelled with a micro-mechanical polymer network model that considers the softening of the elastomer. The network evolution concept used in the micro-mechanical model formulation considers the shorter and longer chain length distribution allowing the softening of material. The moisture diffusion in the material is anomalous behaviour, therefore, the Langmuir-type diffusion model is used to model the moisture diffusion in the crosslinked polymer. The influence of moisture on the mechanical behaviour is modelled by coupling the micro-mechanical network model with the diffusion model. The coupled diffusion and deformation model uses the moisture-dependent mechanical parameter to compute the local parameter for the evaluation of the mechanical behaviour with inhomogeneous moisture distribution. In this paper, crosslinked polyurethane adhesives are used in the numerical investigation of ageing under the influence of moisture with the coupled material model. The experimental investigation for tensile and diffusion behaviours is investigated for different humid conditions at an isothermal condition of 60°C.

1. Introduction

Due to the relatively favourable stress state in glue joints, the glueing technology is predestined for joining thin-walled lightweight structures in vehicle and plant construction. However, the safety-relevant structural bonding of primary structures is generally avoided, as it is not yet possible to calculate the service life of the glue joints under the influence of water or other environmental media. This means that resource-saving lightweight construction potentials are being given away to a large extent. With the increasing use of fibre composite plastics in automotive manufacturing, higher-strength, hyperelastic polyurethane (PU) adhesives with a glass transition temperature of approx. −20°C and a wide glass transition area (up to 60 K) are available, which are very well suited for structural connections of this type. In a similar way, PU adhesives with glass transition are used in the area around 30°C. Understanding the long-term durability of adhesive bonds is a significant research focus because of their viscoelastic behaviour and their sensitivity to the surrounding atmospheric conditions. Therefore, it is necessary to study the effects of environmental conditions on the mechanical behaviour of the adhesive. Recently efforts have been made to study mechanical behaviour under the influence of temperature, and moisture diffusion [1]. In the research, the micromechanical behaviour is not considered in the numerical simulation.

Material models to evaluate viscoelastic behaviour are classified into phenomenological and micromechanical-based network models. The phenomenological model is used to describe the macro mechanical behaviour of the material. These models are formulated from the empirical relation derived from the experimental data and observation but are not supported by theory. The parameters of phenomenological models are identified by fitting the experimental data and have no relevance to the molecular structure of the material. Mooney–Rivlin [2,3], Yeoh [4], and Ogden [5] models are some of the popular phenomenological models based on an invariant or principal stretch of the

* Corresponding author.
E-mail addresses: siva.josyula@uni-saarland.de (S.P. Josyula), s.diebels@mx.uni-saarland.de (S. Diebels).

https://doi.org/10.1016/j.commatsci.2024.113442
Received 27 June 2024; Received in revised form 16 September 2024; Accepted 7 October 2024
Available online 19 October 2024

macroscopic continuum theories. On the contrary, the micromechanical network models are formulated based on the statistical chain mechanics with a motivation to describe the complex micromechanical behaviour. 3-chain model [6,7], the eight-chain model of Arruda and Boyce [8] are the popular material models implemented in commercial finite element programs. A non-affine network model that includes the orientation of chains in the sphere was presented by Miehe et al. [9]. These models idealise the chain distribution of equal lengths and do not consider the softening behaviour of the material.

The microstructure of a crosslinked polymer network is formed of shorter and longer chain distribution, and the shorter chains break/debond at a smaller stretch leading to stress softening [10]. Experiments performed on the crosslinked polymers show stress softening is because of breaking/debonding of the chains of the polymer network [11]. Numerical modelling of the stress-softening behaviour of crosslinked polymer materials has been active research for a long time. Where classical Gaussian or non-Gaussian chain statistics are applied to model the elastic and inelastic behaviour of the polymers. The Gaussian chain statistics uses the end-to-end distance of a single chain formed of a fixed number of chain segments by considering the exact distribution of chain [12]. In comparison, non-Gaussian chain statistics considers a freely joined chain expressed with inverse Langevin function [13]. Govindjee et al. [14], Smeulders et al. [15] proposed a model based on the Arruda-Boyce network model that accounts for the molecular weight distribution to consider the chain length distribution in the polymer network. Marckmann et al. [16] proposed a softening network model by altering the Arruda-Boyce eight-chain network model and considering a mean number of chain segments in a polymer network. Göktepe et al. [17] developed a micromechanical model considering a non-affine approach to include Mullins-type damage due to breakage/debonding of chains in a network. This non-affine micromechanical model is based on the numerical integration scheme proposed by Bazant et al. [18]. In the aforementioned micromechanical softening models, the softening due to damage of the polymer chains is considered with a phenomenological damage function based on the history variables. Dargazany et al. [19] extended the Govindjee et al. [14] model using a numerical integration scheme [18] to include anisotropic behaviour in carbon-filled rubber and softening due to damage in chains is governed by the network evolution. Recently Itskov et al. [20] proposed a full network rubber elasticity and softening model based on the numerical integration over a unit sphere discussed earlier [18]. This model does not consider the filler particles, and the softening behaviour is motivated by the network evolution with an assumption that the distribution of chain segments increases with the maximum stretch.

The present work investigates the finite-strain viscoelastic behaviour of the crosslinked polyurethane adhesive with a softening-based micromechanical model. The micromechanical model is used here to consider the softening of the material with an increase in the stretch. This model considers shorter and longer chain length distribution in a random network of polymer chains. The damage in the chains with an increase in the stretch is modelled based on the network evolution theory. The model discussed here is isotropic and does not include deformation-induced anisotropy. As discussed earlier, the crosslinked polyurethane adhesives are hygroscopic and absorb moisture from the atmosphere causing the material properties to decay, thus leading to early ageing. The ageing in adhesives due to moisture transport is reversible, therefore the chemical ageing of material is not treated in the numerical modelling. Experimental investigation [21] of moisture transport in the crosslinked polyurethane adhesive is anomalous, leading to diffusion of moisture characterised into mobile and immobile moisture concentrations. The anomalous diffusion of moisture is modelled with Langmuir-type diffusion [22]. Numerical investigation of moisture diffusion with the Langmuir-type diffusion model has already been investigated in epoxy-based adhesive [23,24], and these investigations efficiently explain the presence of mobile and immobile moisture concentration in the material domain.

It is necessary to couple the mechanical behaviour with the diffusion behaviour to model the ageing behaviour under the moisture influence. Roy et al. [25] investigated the influence of moisture or solvent diffusion on the non-linear viscoelastic behaviour, where the non-linear Fickian behaviour is taken into consideration, and temperature-dependent diffusion coefficient is used. The influence of diffusion behaviour is investigated on incompressible polymer gels to understand the local rearrangement of molecules due to swelling of gels under large deformations by Hong et al. [26]. Many more coupled material models [27–29] have been developed to investigate the effects of diffusion on the deformation in the polymer gels within the framework of the finite-strain theory. Recently, Goldschmidt et al. [30] have numerically investigated the mechanical behaviour of crosslinked polyurethane under the influence of the humid atmosphere. In which the finite-strain viscoelastic model is coupled with the Fick diffusion using an exponential decay function. Sharma et al. [31] numerically investigated the moisture transport behaviour in polyamide by considering moisture-dependent material properties, and moisture diffusion is modelled using Fick's law. None of the aforementioned theories considers micromechanical and anomalous moisture diffusion behaviour. In the present paper, the proposed micromechanical viscoelastic model is coupled with the Langmuir-type diffusion model and moisture-dependent material parameters of the mechanical model are considered to model ageing behaviour analogous to Sharma et al. [31].

2. Micromechanically motivated polymer free energy

The basic idea of modelling a crosslinked polymer network material involves considering the distribution of shorter and longer chains in a random network. The shorter chains tend to break or debond from the network, leading to the material's softening. This idea is accounted for in the micromechanical material model formulation by multiplying isotropic free energy Ψ of the material with a cumulative distribution function $G(\lambda_m)$

$$W(\mathrm{I}_1, \lambda_c) = \Psi \int_1^{\infty} g(\lambda_m)\mathrm{d}\lambda_m = \Psi G(\lambda_m). \tag{1}$$

The cumulative distribution function considers the break/debonding of the shorter chains following the evolution network theory. In this theory, the shorter chains become inactive as deformation increases, and this process is considered irreversible, contributing to the material's softening. The cumulative distribution function is derived from the probability distribution function defined for a random network. The probability distribution function is defined as a function of the current chain stretch of an ideal chain to evaluate the statistical information concerning the stretch in a random network.

2.1. Polymer chain terminology

An individual chain is formed from N segments of chain links of a uniform length l mm. The end-to-end distance r_0 between endpoints of an ideal chain is arbitrarily calculated as [6,13,32]

$$r_0 = \sqrt{N}l, \tag{2}$$

and the maximum length of chain r_m is calculated as

$$r_m = Nl. \tag{3}$$

The current chain stretch under strained conditions is calculated as

$$r_c = \frac{1}{\sqrt{3}}\sqrt{N}l\sqrt{\mathrm{I}_1}, \tag{4}$$

where I_1 is the first invariant of left Cauchy–Green deformation tensor. Current chain stretch λ_c, and maximum chain stretch $\lambda_{\max}$ are calculated as

$$\lambda_c = \frac{r_c}{r_0} = \frac{\sqrt{\mathrm{I}_1}}{\sqrt{3}}, \quad \text{and} \quad \lambda_{\max} = \frac{r_m}{r_0} = \sqrt{N}. \tag{5}$$

The current chain stretch is defined in the interval between initial chain stretch λ_0 of a rigid chain and maximum $\lambda_{\max}$ chain stretch

$$\lambda_0 = 1 \leq \lambda_c = \frac{\sqrt{\mathrm{I}_1}}{\sqrt{3}} \leq \lambda_{\max}. \tag{6}$$

2.2. Probability distribution function

The maximum chain stretch distribution is defined as analogous to the Wesslau mass distribution function [33] by replacing the mass variable with the actual chain stretch. The Probability distribution function $g(\lambda_m)$ is evaluated from the maximum chain stretch distribution $\mathrm{w}(\lambda_m)$ as

$$\begin{aligned} g(\lambda_m) &= \frac{{}^{N}\lambda_m}{(\lambda_m - 1)}\mathrm{w}(\lambda_m) \\ &= \frac{{}^{N}\lambda_m}{\beta\sqrt{\pi}}\frac{1}{(\lambda_m - 1)^2}\exp\left(\frac{-1}{\beta^2}\left(\ln\left(\frac{(\lambda_m - 1)}{{}^{0}\lambda_m}\right)\right)^2\right). \end{aligned} \tag{7}$$

For simplicity, $g(\lambda_m)$ is rearranged as follows

$$g(\lambda_m) = a_0\frac{1}{(\lambda_m - 1)^2}\exp\left(-a_1\left(\ln\left(a_2(\lambda_m - 1)\right)\right)^2\right) \tag{8}$$

with parameters

$$a_0 = \frac{{}^{N}\lambda_m}{(\beta\sqrt{\pi})};\ a_1 = \frac{1}{\beta^2} \text{ and } a_2 = \frac{1}{{}^{0}\lambda_m}. \tag{9}$$

The constants β, ${}^{0}\lambda_m$ and ${}^{N}\lambda_m$ are calculated with the help of the material parameters polydispersity index Q and average chain elongation ${}^{M}\lambda_m$

$$\beta = \sqrt{2\ln(Q)};\ {}^{N}\lambda_m = \frac{{}^{M}\lambda_m}{Q};\ {}^{0}\lambda_m = \sqrt{{}^{M}\lambda_m\,{}^{N}\lambda_m}. \tag{10}$$

In an unstrained material, every chain actively participates in the free energy of the material. Therefore, the function $g(\lambda_m)$ is integrated between the interval $[1, \infty]$ to compute cumulative distribution function

$$G\left(\lambda_m\right) = \int_1^{\infty} g\left(\lambda_m\right) = 1, \tag{11}$$

where ∞ is the maximum chain stretch λ_m. Softening due to the breaking/debonding of chains in a random network starts with the shorter chains and eventually involves breaking the long chains with a gradual increase in the applied load. Here, a random network is considered to experience a current stretch of λ_c leading to the breaking of shorter chains represented as inactive chains. The other chains that contribute to the mechanical free energy are active. The cumulative distribution function of the active chains under a current stretch λ_c follows the integration of $g\left(\lambda_m\right)$ at an interval $\left[\lambda_c\ \infty\right]$

$$G\left(\lambda_m\right) = \int_{\lambda_c}^{\infty} g\left(\lambda_m\right), \tag{12}$$

where the maximum chain elongation (∞) of a material is a priori unknown quantity, therefore the cumulative density function of the active chains given in Eq. (12) is reformulated by subtracting the cumulative distribution function of the inactive chains from the cumulative distribution function of the unstrained material. As a result, the cumulative distribution function of the active chains follows

$$\begin{aligned} G\left(\lambda_m\right) &= \int_1^{\infty} g(\lambda_m)\mathrm{d}\lambda_m - \int_1^{\lambda_c} g(\lambda_m)\mathrm{d}\lambda_m \\ &= 1 - \int_1^{\lambda_c} g(\lambda_m)\mathrm{d}\lambda_m. \end{aligned} \tag{13}$$

The indefinite integral of the probability density function is evaluated to obtain the cumulative distribution function. After some mathematical evaluation, the cumulative distribution function dependent on λ_m is derived as the function of an error function to avoid non-elementary integrals.

$$G(\lambda_m) = \frac{a_0 a_2 \exp\left(\frac{1}{4a_1}\right)\sqrt{\pi}}{2\sqrt{a_1}}\mathrm{erf}\left(\frac{1 + 2a_1\ln\left(a_2(\lambda_m - 1)\right)}{2\sqrt{\pi}}\right) + C. \tag{14}$$

The integration constant C is determined with an assumption $G(\lambda_m = 1) = 0$ and the error function value as -1 to avoid singularity because of the logarithmic term. As a result, the integration constant is derived as

$$C = \frac{a_0 a_2 \exp\left(\frac{1}{4a_1}\right)\sqrt{\pi}}{2\sqrt{a_1}}, \tag{15}$$

by inserting Eq. (15) in (14) leads to the cumulative density distribution function as:

$$G(\lambda_m) = \frac{a_0 a_2 \exp\left(\frac{1}{4a_1}\right)\sqrt{\pi}}{2\sqrt{a_1}}\left(1 + \mathrm{erf}\left(\frac{1 + 2a_1\ln\left(a_2(\lambda_m - 1)\right)}{2\sqrt{\pi}}\right)\right). \tag{16}$$

After inserting Eq. (13) in (1), the micromechanical free energy density function is derived for a current stretch λ_c in a random network as

$$\begin{aligned} W(\mathrm{I}_1, \lambda_c) &= \Psi(\mathrm{I}_1)\left(\int_1^{\infty} g(\lambda_m)\mathrm{d}\lambda_m - \int_1^{\lambda_c(\mathrm{I}_1)} g(\lambda_m)\mathrm{d}\lambda_m\right) \\ &= \Psi(\mathrm{I}_1)\left(1 - \int_1^{\lambda_c(\mathrm{I}_1)} g(\lambda_m)\mathrm{d}\lambda_m\right), \end{aligned} \tag{17}$$

where Neo-Hooke model is considered as a free energy $\Psi(\mathrm{I}_1)$ in softening micromechanical model for simplicity. However, the crosslinked polyurethane adhesive shows a nearly incompressible viscoelastic behaviour. Therefore, the energy function (17) is uniquely decoupled into volume and shape-changing parts based on the continuum mechanical description [34,35], to further extend the defined material model for analysing finite-strain viscoelastic behaviour. The detailed description of the mechanical energy and the constitutive equation are explained in Appendices A and B

3. Coupled material model

The micromechanical network model is extended to viscoelastic behaviour using a rheological description consisting of Maxwell elements connected in parallel to the spring element (see Fig. 1). The deformation in the body is calculated based on the continuum mechanics of finite-strain theory [36].

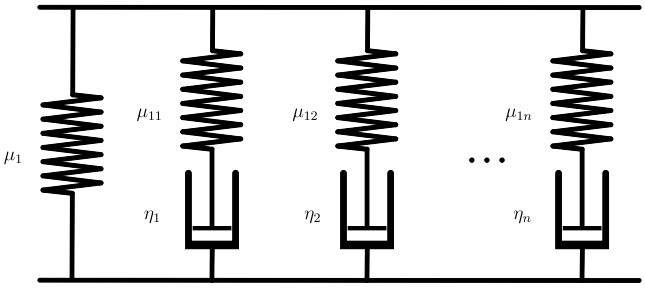

Fig. 1. Rheological model of the viscoelasticity with n Maxwell elements.

3.1. Kinetics of finite-strain theory

The deformation gradient tensor $\mathbf{F}$ needs to be decomposed into elastic $\mathbf{F}_e^j$ and inelastic $\mathbf{F}_i^j$ deformation gradient tensor of $j = 1, \ldots, n$ Maxwell element [37] to model the viscoelastic material model. The deformation tensor is decomposed with multiplicative decomposition

$$\mathbf{F} = \mathbf{F}_e^j \cdot \mathbf{F}_i^j. \tag{18}$$

The free energy is decomposed into shape and volume-changing parts to model a nearly incompressible viscoelastic behaviour. This additive decomposition of free energy leads to multiplicative decomposition of the deformation gradient tensor $\mathbf{F}$ into shape and volume-changing parts and is given as

$$\mathbf{F} = \mathbf{F}_{\text{vol}} \cdot \mathbf{F}_{\text{iso}}, \tag{19}$$

where $\mathbf{F}_{\text{vol}}$ as volumetric part and $\mathbf{F}_{\text{iso}}$ as the isochoric part of the deformation gradient tensor. The volumetric $\mathbf{F}_{\text{vol}}$ and isochoric $\mathbf{F}_{\text{iso}}$ parts of the deformation tensor is calculated as [38]

$$\mathbf{F}_{\text{iso}} = J^{-1/3}\mathbf{F}, \qquad \mathbf{F}_{\text{vol}} = J^{1/3}\mathbf{I} \tag{20}$$

with the Jacobian $J = \det \mathbf{F}$ and second-order identity tensor $\mathbf{I}$. The right Cauchy–Green deformation tensor $\mathbf{C} = \mathbf{F}^T \cdot \mathbf{F}$ is reformulated to isochoric right Cauchy–Green deformation tensor $\bar{\mathbf{C}}$ as $\bar{\mathbf{C}} = J^{-2/3}\mathbf{C}$ from the isochoric deformation gradient tensor given in Eq. (20) [35]. The first I_1 and third I_3 invariants of the Cauchy–Green deformation tensor are calculated as

$$\mathrm{I}_1 = \mathrm{tr}\,(\mathbf{C}) = \mathrm{tr}\,(\mathbf{B})\,;\ \mathrm{I}_3 = \det(\mathbf{C}) = \det(\mathbf{B}) = J^2, \tag{21}$$

where $\mathbf{B} = \mathbf{F} \cdot \mathbf{F}^T$ is the left Cauchy–Green deformation tensor. The counterparts of the invariants are calculated as

$$\bar{\mathrm{I}}_1 = J^{-2/3}\mathrm{I}_1 \qquad \text{and} \qquad \bar{\mathrm{I}}_3 = 1 \tag{22}$$

By combining Eqs. (18), (19) and (20), the kinetics of the elastic part of the Maxwell element is formulated as

$$\bar{\mathbf{B}}_e^j = (\mathbf{F}_e^j)^{(\text{iso})} \cdot ((\mathbf{F}_e^j)^{(\text{iso})})^T = \mathbf{F}_{\text{iso}} \cdot (\bar{\mathbf{C}}_i^j)^{-1} \cdot \mathbf{F}_{\text{iso}}^T. \tag{23}$$

3.2. Thermodynamic consistency

The mechanical behaviour of polyurethane adhesive is dependent on the material's moisture transport. Therefore, the free energy is additively decomposed into the mechanical and diffusion parts, W_{mech} and W_m

$$W = W_{\text{mech}}\left(J, \mathrm{I}_1^{\bar{\mathbf{B}}}, \mathrm{I}_1^{\bar{\mathbf{B}}_e^j}, \lambda_m, m\right) + W_m(m, m_b). \tag{24}$$

Polyurethane adhesive is considered a nearly incompressible material because of the volumetric strains, therefore an uncoupled response is considered to define the free energy function [39,40]. The uncoupled mechanical response is based on the additive decomposition of the free energy into the volumetric and isochoric parts. The isochoric part considers the equilibrium part and the rate-dependent non-equilibrium part. The moisture-dependent function is expressed as

$$W_{\text{mech}} = W_{\text{vol}}\left(J, \lambda_m, m\right) + W_{\text{eq}}\left(\bar{\mathrm{I}}_1^{\bar{\mathbf{B}}}, \lambda_m, m\right) + \sum_{j=1}^{n} W_{\text{neq}}^j\left(\mathrm{I}_1^{\bar{\mathbf{B}}_e^j}, \lambda_m, m\right), \tag{25}$$

where W_{vol} is the volumetric free energy and W_{eq} and W_{neq}^j are the equilibrium and the non-equilibrium parts of the isochoric part. The non-equilibrium part is comprised of $j = 1, 2, \ldots, n$ Maxwell elements. After substituting Eq. (25) leads to the coupled free energy

$$\begin{aligned} W = \quad & W_{\text{vol}}(J, \lambda_m, m) \quad + \quad W_{\text{eq}}\left(\mathrm{I}_1^{\bar{\mathbf{B}}}, \lambda_m, m\right) \\ & + \sum_{j=1}^{n} W_{\text{neq}}^j\left(\mathrm{I}_1^{\bar{\mathbf{B}}_e^j}, \lambda_m, m\right) \quad + \quad W_m(m, m_b). \end{aligned} \tag{26}$$

An important requirement for the material model is to satisfy the Clausius–Planck inequality. The Clausius–Planck inequality for the coupled diffusion and mechanical behaviours at the isothermal condition follows

$$\rho\dot{W} - \mathbf{T} : \mathbf{D} + \mathrm{div}\left(R_m \mathbf{q}\right) \geq 0, \tag{27}$$

where R_m is the chemical potential and $\mathbf{q}$ is the moisture flux. The process variables for the defined coupled material model are

$$\mathcal{S} = \left\{\mathbf{B}, \mathbf{B}_e^j, m, \mathrm{grad}\, m\right\}, \tag{28}$$

and the constitutive quantities are

$$\mathcal{R} = \{W, \mathbf{T}, \mathbf{q}\}. \tag{29}$$

The material time derivative of the free energy function is derived with the process variable to evaluate dissipation as

$$\begin{aligned} \dot{W} = & \frac{\partial W_{\text{vol}}(J, \lambda_m, m)}{\partial \bar{\mathbf{B}}} : \dot{\mathbf{B}} + \frac{\partial W_{\text{eq}}\left(\mathrm{I}_1^{\bar{\mathbf{B}}}, \lambda_m, m\right)}{\partial \bar{\mathbf{B}}} : \dot{\mathbf{B}} + \\ & \sum_{j=1}^{n} \frac{\partial W_{\text{neq}}^j\left(\mathrm{I}_1^{\bar{\mathbf{B}}_e^j}, \lambda_m, m\right)}{\partial \bar{\mathbf{B}}_e^j} : \dot{\mathbf{B}}_e^j + \frac{\partial W_m\left(m, m_b\right)}{\partial m} : \dot{m}. \end{aligned} \tag{30}$$

The time derivatives of the deformation tensors are formulated with the deformation velocity $\mathbf{D}$ as

$$\dot{\mathbf{B}} = 2\mathbf{D} \cdot \mathbf{B} \quad \text{and} \quad \dot{\mathbf{B}}_e^j = 2\mathbf{D} \cdot \mathbf{B}_e^j - 2\mathbf{F}_e^j \cdot \hat{\mathbf{\Gamma}}_i^j \cdot \left(\mathbf{F}_e^j\right)^T, \tag{31}$$

where the inelastic deformation rate of the intermediate configuration $\hat{\mathbf{\Gamma}}_i^j$ is an outcome of the product rule applied over $\dot{\mathbf{B}}_e^j$. The Clausius–Planck inequality is derived with the material time derivative of the free energy (30) and the time derivatives of the deformation tensor as

$$\begin{aligned} & \left(-2\rho\mathbf{B} \cdot \frac{\partial W_{\text{vol}}}{\partial \mathbf{B}} - 2\rho\mathbf{B} \cdot \frac{\partial W_{\text{eq}}}{\partial \mathbf{B}} - \sum_{j=1}^{n} 2\rho\bar{\mathbf{B}}_e^j \cdot \frac{\partial W_{\text{neq}}}{\partial \bar{\mathbf{B}}_e^j} + \mathbf{T}\right) : \mathbf{D} \\ & + \sum_{j=1}^{n} 2\rho \frac{\partial W_{\text{neq}}}{\partial \bar{\mathbf{B}}_e^j} : \left(\mathbf{F}_e^j \cdot \hat{\mathbf{\Gamma}}_i^j \cdot \left(\mathbf{F}_e^j\right)^T\right) + \left(-\rho \frac{\partial W_m(m, m_b)}{\partial m} + R_m\right) \cdot \dot{m} \\ & - \mathrm{grad}\, R_m \cdot \mathbf{q} \geq 0. \end{aligned} \tag{32}$$

The inequality (32) depends linearly on the independent variables $\mathbf{D}$, $\dot{m}$. Thus leading to the stress and the diffusion potential from Coleman and Noll [41] argumentation

$$\begin{aligned} \mathbf{T} &= 2\rho\mathbf{B} \cdot \frac{\partial W_{\text{vol}}}{\partial \mathbf{B}} + 2\rho\mathbf{B} \cdot \frac{\partial W_{\text{eq}}}{\partial \mathbf{B}} + \sum_{j=1}^{n} 2\rho\bar{\mathbf{B}}_e^j \cdot \frac{\partial W_{\text{neq}}^j}{\partial \bar{\mathbf{B}}_e^j}, \\ R_m &= \rho \frac{\partial W_m(m, m_b)}{\partial m}. \end{aligned} \tag{33}$$

The first term of the stress tensor represents the volumetric stress analogues to the hydrostatic stress [40], and the other two terms correspond to the equilibrium and non-equilibrium parts. Applying the chain rule to the volumetric stress component with the relationship $\partial J / \partial \mathbf{B} = J\mathbf{B}^{-1}$ and assuming $W_{(\bullet)} = \rho W_{(\bullet)}$ [39] leads to the stress tensor

$$\mathbf{T} = JW_{\text{vol}}'\mathbf{I} + 2\mathbf{B} \cdot \frac{\partial W_{\text{eq}}}{\partial \mathbf{B}} + \sum_{j=1}^{n} 2\bar{\mathbf{B}}_e^j \cdot \frac{\partial W_{\text{neq}}^j}{\partial \bar{\mathbf{B}}_e^j}, \tag{34}$$

where $W_{\text{vol}}' = \partial W_{\text{vol}} / \partial J$. The dissipation inequality is simplified to

$$\sum_{j=1}^{n} 2\rho \frac{\partial W_{\text{neq}}^j\left(\mathrm{I}_1^{\mathbf{B}_e^j}, m\right)}{\partial \bar{\mathbf{B}}_e^j} : \left(\mathbf{F}_e^j \cdot \hat{\mathbf{\Gamma}}_i^j \cdot \left(\mathbf{F}_e^j\right)^T\right) - \mathrm{grad} R_m \cdot \mathbf{q} \geq 0. \tag{35}$$

Using the kinematic relations and applying tensor relations, the first term of the dissipation inequality of Eq. (35) results in the evolution equation of the right Cauchy–Green deformation [36,42,43]

$$\dot{\bar{\mathbf{C}}}_i^j = \frac{4}{r_j}\left[\bar{\mathbf{C}} - \frac{1}{3}\mathrm{tr}\left(\bar{\mathbf{C}} \cdot \left(\bar{\mathbf{C}}_i^j\right)^{-1}\right)\bar{\mathbf{C}}_i^j\right] \tag{36}$$

where r_j is the relaxation time associated with jth Maxwell element. The relaxation times are the material constants introduced as

$$r_j = \frac{\mu_{10n}}{\eta_n}. \tag{37}$$

The second term is characterised by the diffusive flux to ensure the positivity of the simplified dissipation inequality

$$\mathbf{q} = -D\left(\mathrm{grad}\, R_m\right), \tag{38}$$

where D is the diffusion coefficient. Free energy of the moisture diffusion $W_m(m, m_b)$ is defined for the anomalous moisture diffusion as

$$W_m(m, m_b) = \frac{1}{2}\left(m - m_b\right)^2, \tag{39}$$

where m and m_b are the total and immobile moisture concentrations. The chemical potential equation derived in Eq. (33), diffusive flux (38), the diffusion free energy Eq. (39) and the balance of mass [44] leads to the anomalous diffusion equation

$$\frac{\mathrm{d}m}{\mathrm{d}t} = D\,\mathrm{div}\left(\mathrm{grad}\,(m - m_b)\right), \tag{40}$$

and the immobile moisture concentration m_b is calculated with an evolution equation [22]

$$\dot{m_b} = \alpha m_f - \beta m_b. \tag{41}$$

The symbol α is a material parameter that amounts to the rate at which the mobile moisture becomes immobile, and β represents the rate at which the immobile moisture becomes mobile. The Langmuir-type diffusion is discussed in detail in Appendix C

4. Governing partial differential equations

The governing equations of the coupled material model expressed in the deformed consist of the balance of momentum to express mechanical behaviour and the Langmuir-type diffusion model to express moisture diffusion

$$\begin{aligned} \mathrm{div}\,\mathbf{T}\left(J, \bar{\mathbf{B}}, \bar{\mathbf{B}}_e^j, m\right) &= \mathbf{0} \quad \forall \quad \mathbf{x} \in \Omega, \text{ and} \\ \dot{m} = D\,\Delta m_f = D\,\mathrm{div}\left(\mathrm{grad}\left(m - m_b\right)\right) &\quad \forall \quad \mathbf{x} \in \Omega, \end{aligned} \tag{42}$$

where the moisture-dependent Cauchy stress tensor $\mathbf{T}$ is expressed as

$$\mathbf{T} = \mathbf{T}_{\mathrm{vol}}(J, \lambda_m, m) + \mathbf{T}_{\mathrm{eq}}(\bar{\mathbf{B}}, \lambda_m, m) + \sum_{j=1}^{n} \mathbf{T}^j_{\mathrm{neq}}(\mathbf{B}^j_e, \lambda_m, m). \tag{43}$$

The Cauchy stress is calculated using stiffness parameters that depend on the local moisture concentration, to evaluate the ageing behaviour. The moisture-dependent stiffness parameters are calculated by interpolating the dry and saturated states of the material [31]. The interpolation is given by

$$\mu(m) = f(m)\mu^{\mathrm{dry}} + (1 - f(m))\mu^{\mathrm{sat}}, \tag{44}$$

where $\mu(m)$ is the local stiffness parameters calculated at the integration points. μ^{dry} and μ^{sat} are the stiffness parameters of dry and saturated material samples. $f(m)$ is an interpolation function to couple mechanical and diffusion equations. The coupling function is defined using an exponential decay

$$f(m) = \exp(-\Lambda m), \tag{45}$$

where Λ is a parameter of the decay function. The coupling function has to satisfy the condition $0 \leq f(m) \leq 1$, where $f(m) = 1$ defines a dry state and $f(m) \approx 0$ defines a saturated state.

4.1. Boundary and initial conditions

The initial and boundary conditions are needed for the defined governing equations of the coupled system of equations. The initial conditions are defined over the material domain to solve the Langmuir-type diffusion model. Total moisture and immobile moisture distribution in the material at time $t_0 = 0$ is applied as the initial boundary condition

$$m\,(\mathbf{x}, t = 0) = 0, \quad m_b\,(\mathbf{x}, t = 0) = 0. \tag{46}$$

Let Dirichlet and Neumann boundaries for the moisture diffusion are $\partial\Omega_D$ and $\partial\Omega_N$ and the mechanical problem are $\partial\Omega^D_{\mathbf{u}}$ and $\partial\Omega^N_{\mathbf{u}}$ and has to satisfy

$$\begin{aligned} \partial\Omega_N \cup \partial\Omega_D &= \partial\Omega, \quad \partial\Omega_N \cap \partial\Omega_D = \varnothing \\ \partial\Omega^D_{\mathbf{u}} \cup \partial\Omega^N_{\mathbf{u}} &= \partial\Omega, \quad \partial\Omega^D_{\mathbf{u}} \cap \partial\Omega^N_{\mathbf{u}} = \varnothing \end{aligned} \tag{47}$$

The diffusion and deformation boundary conditions are defined over the specified Dirichlet and Neumann boundaries as follows

$$\begin{aligned} &\mathbf{u}\,(\mathbf{x}, t) = \mathbf{u}_D\,(\mathbf{x}, t) \text{ on } \partial\Omega^D_{\mathbf{u}} \text{ and } \mathbf{T}\cdot\mathbf{n} = \mathbf{t} \text{ on } \partial\Omega^N_{\mathbf{t}}, \\ &m\,(m(\mathbf{x}, t)) = m^{\mathrm{eq}} \;\forall\; \mathbf{x} \in \partial\Omega^D_m \text{ and } \mathbf{q}\,(\mathbf{x}, t) = D\,\mathrm{grad} m_f \cdot \mathbf{n} \;\forall\; \mathbf{x} \in \partial\Omega^N_{\mathbf{q}}. \end{aligned} \tag{48}$$

where $\mathbf{t}$ is the traction on the surface $\partial\Omega^N_{\mathbf{t}}$ with the normal vector $\mathbf{n}$, m^{eq} is the relative humidity in the surrounding atmosphere and n is the outward normal vector on the boundary. The coupled problem is implemented and solved in deal.II finite element library [45–47]. The displacement and diffusion fields of the coupled problem are solved individually as a coupled staggered field to obtain a stable implicit formulation.

5. Numerical implementation and investigation

The weak forms of the governing equations are derived to solve the partial differential equations defined in Section 4 using the finite element method. To this end, the arbitrary test functions $\delta\mathbf{u}$ are δm are multiplied by the governing equations and are integrated over the material volume

$$\begin{aligned} \int_\Omega \delta\mathbf{u}\cdot\mathrm{div}\,\mathbf{T}\left(\bar{\mathbf{B}}, \bar{\mathbf{B}}^j_e, J, m\right)\mathrm{dV} &= \mathbf{0}, \\ \int_\Omega \delta m\,\dot{m}\mathrm{dV} - \int_\Omega \delta m\, D\,\mathrm{div}\left(\mathrm{grad}\left(m - m_b\right)\right)\mathrm{dV} &= 0. \end{aligned} \tag{49}$$

Finally, integration by parts leads to

$$\begin{aligned} \mathbf{r}_{\mathbf{u}}(\mathbf{u}) &= \int_\Omega \mathbf{T}\left(\bar{\mathbf{B}}, \bar{\mathbf{B}}^j_e, J, m\right) : \mathrm{grad}^s\,\delta\mathbf{u}\,\mathrm{dV} - \int_{\partial\Omega} \mathbf{T}\cdot\delta\mathbf{u}\,\mathrm{dA} = \mathbf{0}, \\ \mathrm{r}_m(m) &= \int_\Omega \delta m\,\dot{m}\,\mathrm{dV} + \int_\Omega \left[\mathrm{grad}\delta m\cdot D\,\mathrm{grad}\left(m - m_b\right)\right]\mathrm{dV} = 0. \end{aligned} \tag{50}$$

Diffusion is a long-term process for a material to reach equilibrium. Therefore, the diffusion equation needs to consider larger time steps to solve the problem with less computational effort. The Crank–Nicolson method [48], which uses a second-order time derivative, is employed to solve the diffusion problem, as both explicit and implicit time derivatives have temporal truncation errors for larger time steps [49]. The time discretisation with the Crank–Nicolson method leads to the residual $\mathrm{r}_m(m)$

$$\begin{aligned} \mathrm{r}_m(m) = \int_\Omega \delta m\,\frac{m^{t+1} - m^t}{\Delta t}\mathrm{dV} &+ \int_\Omega \left[\mathrm{grad}\delta m\cdot D\,\frac{1}{2}\mathrm{grad}\left(m^{t+1} - m_b^{t+1}\right)\right]\mathrm{dV} \\ &- \int_\Omega \left[\mathrm{grad}\delta m\cdot D\,\frac{1}{2}\mathrm{grad}\left(m^{t} - m_b^{t}\right)\right]\mathrm{dV} = 0, \end{aligned} \tag{51}$$

where $(\bullet)^{t+1}$ and $(\bullet)^t$ are the values of the field variables calculated at current time $t + 1$ s and previous time t s steps. The evolution Eq. (41) is solved to evaluate the immobile moisture concentration as

$$\frac{m_b^{t+1} - m_b^t}{\Delta t} = \frac{1}{2}\left[\alpha\left(m^{t+1} - m^t\right)\right] - \frac{1}{2}\left[(\alpha + \beta)\left(m_b^{t+1} - m_b^t\right)\right]. \tag{52}$$

The differential equation is treated to consider the geometrical non-linearity because of the large deformations. The linearised approximation of the non-linear governing equations is solved with Newton's method using

$$\mathbf{R}\,(\Xi + \Delta\Xi) \approx \mathbf{R}(\Xi) + \mathrm{D}_{\Delta\Xi}\mathbf{R}\,(\Xi)\cdot\mathrm{d}\Xi = 0, \tag{53}$$

where $\mathrm{D}_{\Delta\Xi}(\bullet)$ represents the directional derivative, also known as the spatial tangent tensor, that describes the change in the residuals $\mathbf{R}(\Xi)$ in the direction of the unknown vector Ξ. The component of the directional derivative $\mathbf{K}^{mm}$ known as the diffusive matrix is

$$\mathbf{K}^{mm} = \int_\Omega \mathrm{grad}\,\delta m\,\mathrm{grad}\,\delta m\,\mathrm{dV}, \tag{54}$$

and the direction derivative component $\mathbf{K}^{\mathbf{uu}}$ in the direction $\Delta\mathbf{u}$ is

$$\begin{aligned} \mathbf{K}^{\mathbf{uu}} = \mathrm{D}_{\Delta\mathbf{u}}\mathbf{r}(\mathbf{u}) = \int_\Omega \mathrm{D}_{\Delta\mathbf{u}}\left(\mathbf{T}\left(\bar{\mathbf{B}}, \bar{\mathbf{B}}^j_e, J, m\right)\right) : \mathrm{grad}^s\,\delta\mathbf{u}\,\mathrm{dV} \\ + \int_\Omega \mathbf{T}\left(\bar{\mathbf{B}}, \bar{\mathbf{B}}^j_e, J, m\right) : \left[\mathrm{Grad}\,\delta\mathbf{u}\cdot\mathrm{D}_{\Delta\mathbf{u}}\mathbf{F}^{-1}\right]\mathrm{dV}, \end{aligned} \tag{55}$$

the directional derivative $\mathbf{K}^{\mathbf{uu}}$ is simplified to

$$\mathbf{K}^{\mathbf{uu}} = \mathrm{D}_{\Delta\mathbf{u}}\mathbf{r}(\mathbf{u}) = \int_{\Omega} \mathrm{grad}^{s}\,\Delta\mathbf{u} : \overset{4}{\boldsymbol{\kappa}}\left(\bar{\mathbf{B}}, \bar{\mathbf{B}}_{e}^{j}, J, m\right) : \mathrm{grad}^{s}\,\delta\mathbf{u}\,\mathrm{dV} + \int_{\Omega} \mathrm{grad}\,\delta\mathbf{u} : \left[\mathrm{grad}\,\Delta\mathbf{u}\cdot\mathbf{T}\left(\bar{\mathbf{B}}, \bar{\mathbf{B}}_{e}^{j}, J, m\right)\right]\mathrm{dV}. \tag{56}$$

Here, the tangent $\overset{4}{\boldsymbol{\kappa}}$ is calculated as the sum of the volumetric $\overset{4}{\boldsymbol{\kappa}}_{\mathrm{vol}}$ and isochoric components composing of the equilibrium $\overset{4}{\boldsymbol{\kappa}}_{\mathrm{eq}}\left(\bar{\mathbf{B}}, m\right)$ and $j = 1, 2, \ldots, n$ non-equilibrium $\overset{4}{\boldsymbol{\kappa}}_{\mathrm{neq}}\left(\bar{\mathbf{B}}_{e}^{j}, m\right)$ parts of the viscoelastic model. The Eq. (B.4) in the Appendix defines the tangent matrices. $\bar{\mathbf{B}}_{e}^{j}$ of the jth non-equilibrium part is calculated from the evolution equation of the inelastic right Cauchy–Green deformation tensor $\bar{\mathbf{C}}_{i}^{j}$. This evolution equation is solved with the implicit Euler method in time combined with the local Newton method in space at every integration point.

The parameters of the mechanical and diffusion models are identified by fitting simulation curves to the experimental curves. A gradient-free method proposed by Nelder & Mead [50] is used for parameter identification. At first, the Langmuir-type diffusion parameters are identified from the gravimetric tests conducted with 98% r.H. in the atmosphere at an isothermal condition of 60 °C. Then, the viscoelastic behaviour is studied with the uniaxial tensile tests performed on the dry and aged samples at an isothermal condition. The corresponding material parameters of the micromechanical model are identified for dry and aged samples. The micromechanical model parameters of dry and aged samples are evaluated to define the decay function to interpolate the material parameters to analyse the ageing behaviour.

5.1. Diffusion

A thin sample of 0.833 mm thick sample is used to investigate the moisture diffusion in the polyurethane adhesive. The top and bottom faces along the thickness are exposed to moisture, while the other faces are isolated from the surroundings, ensuring that the moisture diffusion is one-dimensional. The Langmuir-type diffusion model parameters are identified with the curve fitting process. The optimum material parameters are listed in Table 1.

Table 1
Langmuir-type diffusion parameters obtained from curve fitting method.

Diffusion parameters at 60 °C	
Diffusion coefficient D	7.925E − 05 mm^2 s^{-1}
Rate at which immobile moisture becomes mobile again α	2.727E − 05 s^{-1}
Rate at which mobile moisture becomes immobile β	2.247E − 03 s^{-1}

The experimental and simulation results are plotted together to check for the deviation between the results (see Fig. 2).

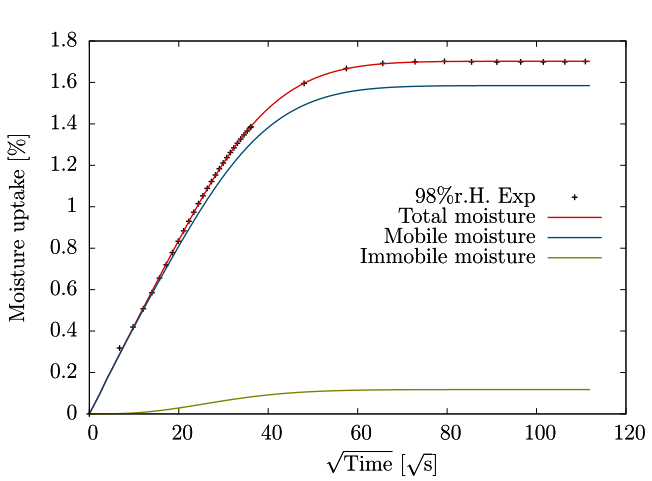

Fig. 2. Comparison between experimental (Exp) and simulation data of moisture absorption at 60 °C with 98% relative humidity in air.

The total moisture concentration calculated with the material properties given in Table 1 shows good agreement with the experimental results.

5.2. Material parameters of micromechanical model

The viscoelastic behaviour of the crosslinked adhesive under the influence of moisture is investigated by performing a uniaxial tensile test. The test sample is optimised to have a minimum cross-section at the centre Fig. 3. The motivation to use a tailored sample is to measure local strains at 2 mm span from the centre of the specimen. These tailored samples are not subjected to any pre-stressed or strains in the manufacturing process.

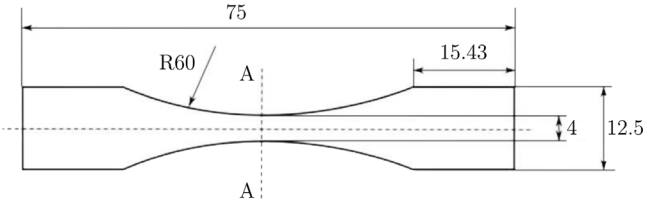

Fig. 3. Tailored tensile test samples with a necked cross-section at the centre of the sample: all dimensions are in millimetres.

The samples are aged at different humid (0% r.H., 29% r.H., 67% r.H., 100% r.H.) conditions at an isothermal condition of 60 °C to investigate the moisture influence on the tensile strength. Seven Maxwell elements are used to model the viscoelastic behaviour.

The finite element model is applied with the tensile boundary conditions with the micromechanical material parameters listed in Table 2 for different atmospheric conditions.

The finite element analysis performed with the optimal parameters is compared with the test results. Fig. 4 shows the comparison of stress–stretch data between simulation and test results with the standard deviation. The tension test data plotted in the comparison corresponds to the mean values calculated from the test series consisting of five samples for aged samples at individual humid climatic conditions. The standard deviation in the form of the error bar indicates that the problem is well-posed.

It is apparent from the uniaxial tensile test that the tensile strength decreases with an increase in moisture concentration due to the decrease in the material stiffness. The stiffness parameters decrease exponentially with an increase in the local moisture concentration. Decay in the stiffness parameters is estimated by interpolating parameters as the function of moisture concentration [31]. The moisture-dependent stiffness parameters are calculated at integration points with Eq. (44). Dry μ^{dry} and saturated μ^{sat} at 100% r.H. stiffness parameters listed in Table 2 are used in the interpolation. The coupling parameter Λ of the integration function $f(m)$ given in Eq. (45) is identified as $\Lambda = 2.16$. The decay of the exponentiak function for the moisture uptake is shown in Fig. 5, represnting the dry and saturated states.

6. Investigation of coupled problem

Multi-physically coupled diffusion and deformation model is quantified by investigating the tailored sample with inhomogeneous moisture distribution. The sample is investigated for different ageing times exposed to 100% r.H. atmospheric conditions. The aged samples for different times are applied with the tensile boundary conditions inconsistent with the uni-axial tensile tests. The stress–stretch data is measured locally at a span of 2 mm from the centre of the sample. For finite element analysis, the moisture is diffused from two end faces of the sample for time t = 4000 s, 10000 s, 15000 s and 60000 s to prepare aged samples with inhomogeneous moisture distribution. The aged samples are applied with the tensile test boundary condition. Fig. 6 shows the schematic representation of the applied boundary conditions.

Table 2
Material parameters of micromechanical polymer network model at different ambient condition.

Material parameters of micromechanical model						
		Relaxation times [s]	0% r.H.	29% r.H.	67% r.H.	100% r.H.
Equilibrium	c_{10} [MPa]		9.183	7.744	6.455	6.052
Non-equilibrium	c_{101} [MPa]	0.5	5.223	4.654	4.225	4.044
	c_{102} [MPa]	10	4.152	3.654	3.225	3.044
	c_{103} [MPa]	100	3.140	2.654	2.225	2.144
	c_{104} [MPa]	500	2.328	1.543	1.035	1.012
	c_{105} [MPa]	1000	1.582	1.317	0.618	0.404
	c_{106} [MPa]	2500	1.131	1.068	0.326	0.246
	c_{107} [MPa]	5000	0.961	0.778	0.686	0.107
Wesslau parameters	Average chain stretch ${}^{M}\lambda_m$		1.194	1.287	1.658	1.931
	Polydispersity index Q		1.001	1.039	1.272	1.367

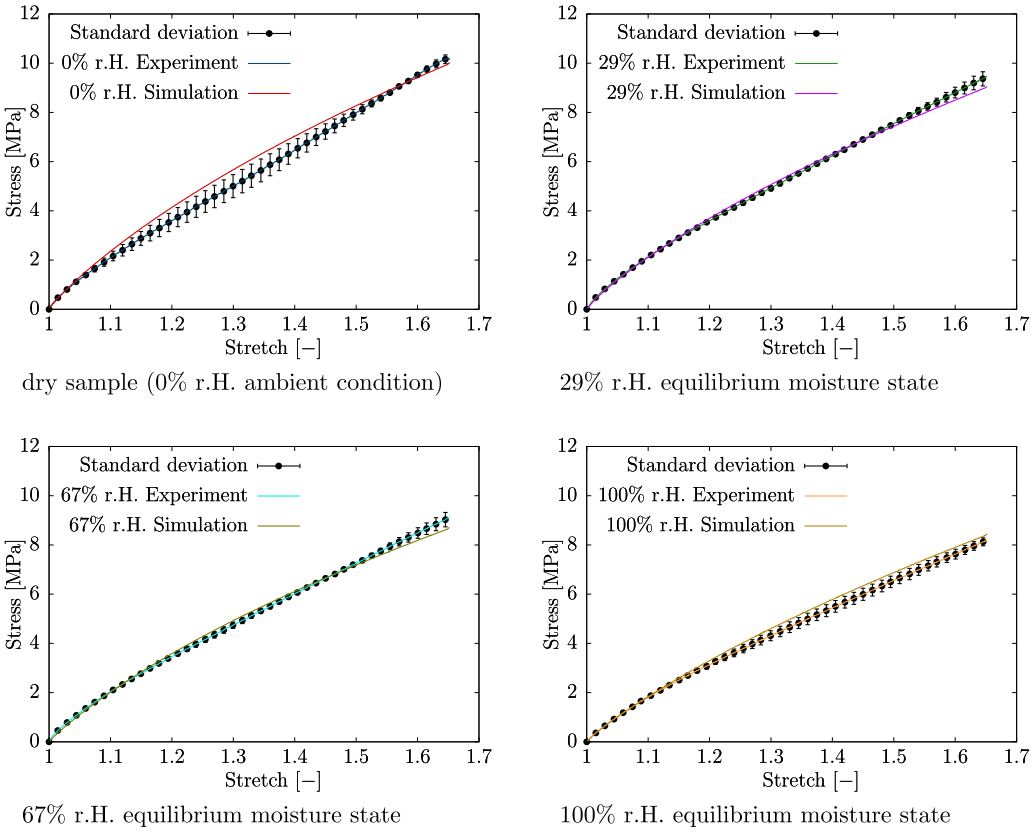

Fig. 4. Curve fitting of simulation data with experimental data under tensile test at different ambient moisture conditions at 60 °C.

The coupled problem is solved by first addressing the diffusion problem and then superimposing the moisture distribution on the mechanical model to evaluate local mechanical parameters. Consequently, the 2 mm cross-section model is spatially discretized and the diffusion material parameters listed in Table 1 are applied to prepare aged samples for different time intervals. Fig. 7 shows a comparison of moisture distribution along the centre of the sample at different times. Results indicate that the concentration of moisture molecules diffused in the sample increases with time and finally reaches an equilibrium state.

The stiffness parameters at the integration points are calculated with dry and saturated parameters listed in Table 2 using Eq. (44). The experimental stretch–stress curves of dry and at 100% r.H. saturated samples are plotted against the simulation results to validate the coupled material model. It is evident from Fig. 8 that the loss in the stiffness parameters with increasing moisture concentration results in lower tensile strength. The sample reaches the equilibrium at time $t = 60,000$ s, and the simulation results coincide with the test results of the sample aged at 100% r.H. The simulation results of the sample with inhomogeneous moisture distribution fall between the dry and 100% r.H. aged samples validating the proposed coupled material model.

7. Summary and future work

Many recent works have been carried out to develop a coupled material model to investigate the ageing behaviour of crosslinked polymers. In this paper, crosslinked polyurethane adhesives are used to examine the influence of moisture on mechanical behaviour. These combined material models, which integrate the phenomenological model with Fick's diffusion model, are not suitable for studying the ageing behaviour of crosslinked polyurethane adhesives. Therefore, a

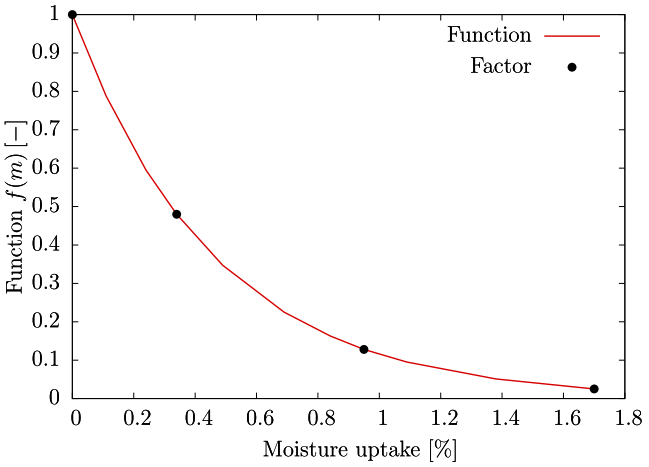

Fig. 5. Exponential decay function to interpolate the material parameters.

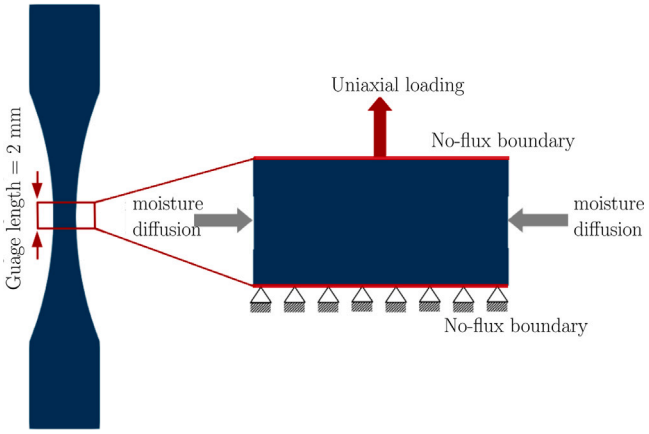

Fig. 6. Left and right faces of 2 mm wide cross-section of the tailored tensile sample is subject to moisture diffusion for time t s with no-flux boundaries and then the sample is uniaxially loaded with a strain rate of $0.0005\,s^{-1}$.

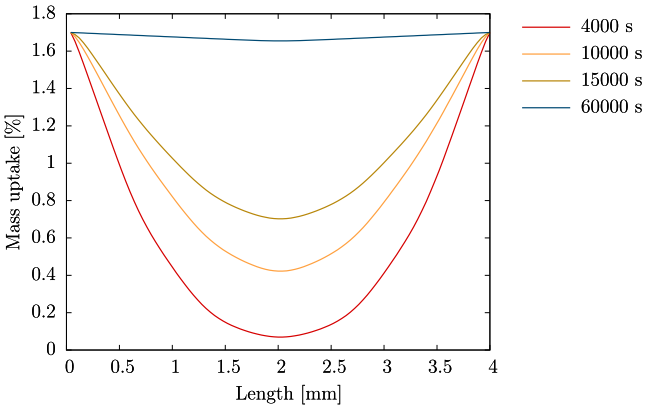

Fig. 7. Distribution of moisture over the cross-section of the adhesive sample determined by simulation at different times.

micro-mechanical model is developed and discussed in detail to investigate the rate-dependent mechanical behaviour. The micro-mechanical model relies on the statistical analysis of polymer network chains considering shorter and longer chain length distributions. Wesslau distribution function is used to define the distribution of chains as a function of maximum chain elongation. The distribution function evaluates the softening behaviour of material due to the damage/debonding of shorter chains with an increase in chain elongation. The micro-mechanical model is extended to rate-dependent mechanical behaviour by combining spring and Maxwell elements in parallel. In the current work, seven Maxwell elements are used to model the viscoelastic behaviour.

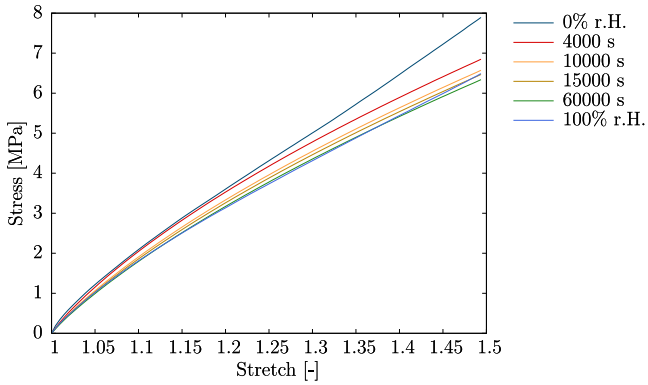

Fig. 8. Comparison of the stress–stretch curves of the samples with inhomogeneous moisture distribution with dry and saturated samples at 100% relative humidity in climate.

The crosslinked polyurethane adhesives exhibit hygroscopic behaviour leading to absorption of moisture from the surrounding atmosphere. Infrared investigations performed on basic polyurethane adhesive to study moisture absorption show anomalous diffusion behaviour. Langmuir-type diffusion model is used to model the anomalous diffusion behaviour classifying the diffused moisture into mobile and immobile moisture concentrations. The micro-mechanical viscoelastic material model is coupled with the Langmuir-type diffusion model to investigate the ageing of material with inhomogeneous moisture distribution. The mechanical and diffusion models are coupled by using moisture-dependent stiffness parameters by assuming constant relaxation times irrespective of the moisture condition.

To investigate the ageing behaviour of crosslinked polyurethane adhesives under various humid conditions at a constant temperature, samples were prepared. Both dry and aged samples were tested for moisture diffusion behaviour and tensile strength. The resulting data were used to determine the necessary parameters for the coupled material model. These parameters were then employed to define the coupling function, which calculates moisture-dependent stiffness parameters at integration points to couple diffusion and viscoelastic models. The coupled material model was validated by comparing the stress–stretch data from the numerical results of samples with inhomogeneous moisture distribution to the tensile test results of saturated samples. The comparison yielded satisfactory results, indicating the model's potential for further improvement

In modelling crosslinked polymers, both Gaussian and inverse Langevin statistics are crucial for investigating material behaviour. The inverse Langevin chain statistics account for the large deformations of the chains. Consequently, the free energy function of the micro-mechanical model needs to incorporate the inverse Langevin chain statistics. In this study, we assume that swelling deformation due to moisture diffusion is negligible, as the time required for the sample to reach saturation is short. However, even a minor swell stretch significantly impacts the resulting stresses, thereby affecting the stiffness parameters of the material model. The plan is to extend the micro-mechanical model to a polymer chain model based on inverse Langevin chain statistics. So far, the coupled material model is formulated to capture one-sided coupling effects, this means that the influence of diffusion on the mechanical behaviour is captured but not the other side. Furthermore, the test to investigate the swell stretch needs to

be performed to extend the coupled model to consider the swelling behaviour in the formulation.

CRediT authorship contribution statement

S.P. Josyula: Writing – review & editing, Writing – original draft, Methodology, Investigation, Conceptualization. **A. Wulf:** Methodology, Conceptualization. **B. Zimmer:** Investigation.

Declaration of competing interest

The authors declare the following financial interests/personal relationships which may be considered as potential competing interests: Siva Pavan Josyula reports financial support was provided by AiF Projekt GmbH. Other authors have no known competing financial interests or personal relationships that could have appeared to influence the work reported in this paper.

Acknowledgments

The research project 19730 *N* "Berechnung des instationären mechanischen Verhaltens von alternden Klebverbindungen unter Einfluss von Wasser auf den Klebstoff" of the research association Forschung svereinigung Stahlanwendung e.V. (FOSTA), Düsseldorf was supported by the Federal Ministry of Economic Affairs and Energy through the AiF as part of the program for promoting industrial cooperative research (IGF) on the basis of a decision by the German Parliament.

Appendix A. Decomposition of micromechanical energy

The softening-based micromechanical model is an extension of the model to model viscoelastic behaviour is discussed in Sections 2 and 3. The decomposition of the viscoelastic free energy into shape and volume-changing parts is discussed in detail to evaluate the constitutive equations.

A.1. Isochoric part of free energy

The invariants of the deformation tensor are necessary for modelling the micromechanical model. As aforementioned, invariants of the isochoric and volumetric parts discussed before being substituted in Eq. (17) to formulate the isochoric part of free energy

$$W_{\text{iso}}(\bar{\mathrm{I}}_1,\lambda_m)=\Psi_{\text{iso}}(\bar{\mathrm{I}}_1)\left(\int_1^{\infty} g_{\text{iso}}(\lambda_m)\mathrm{d}\lambda_m-\int_1^{\lambda_c} g_{\text{iso}}(\lambda_m)\mathrm{d}\lambda_m\right), \tag{A.1}$$

where the isotropic free energy of material Ψ_{iso} is defined with Neo-Hookean model for simplicity [3]. As a result, the isochoric part of the micromechanical free energy is

$$\begin{aligned} W_{\text{iso}}(\bar{\mathrm{I}}_1,\lambda_m)&=c_{10}\left(\bar{\mathrm{I}}_1-3\right)\left(1-\int_1^{\lambda_c} g_{\text{iso}}(\lambda_m)\mathrm{d}\lambda_m\right)\\ &=\Psi_{\text{iso}}(\bar{\mathrm{I}}_1)\left(1-G_{\text{iso}}\left(\lambda_c(\bar{\mathrm{I}}_1)\right)\right). \end{aligned} \tag{A.2}$$

Due to the implicit dependence of $G_{\text{iso}}\left(\lambda_c(\bar{\mathrm{I}}_1)\right)$ on $\lambda_c(\bar{\mathrm{I}}_1)$, the necessary derivatives are computed using the chain rule to derive stress and tangent tensors. With the derivative operators $\frac{\partial(\cdots)}{\partial\lambda_c}=(\dot{\cdots})$ and $\frac{\partial(\cdots)}{\partial\mathrm{I}_1}=(\cdots)'$, the first and second order derivatives are

$$\begin{aligned} G'_{\text{iso}}\left(\lambda_c(\bar{\mathrm{I}}_1)\right)&=\frac{\partial G_{\text{iso}}}{\partial\lambda_c}\frac{\partial\lambda_c}{\partial\bar{\mathrm{I}}_1}=\dot{G}_{\text{iso}}\lambda'_c,\\ G''_{\text{iso}}\left(\lambda_c(\bar{\mathrm{I}}_1)\right)&=\frac{\partial}{\partial\bar{\mathrm{I}}_1}\left(\dot{G}_{\text{iso}}\lambda'_c\right)=\frac{\partial\dot{G}_{\text{iso}}}{\partial\lambda_c}\frac{\partial\lambda_c}{\partial\bar{\mathrm{I}}_1}\lambda'_c+\dot{G}_{\text{iso}}\frac{\partial\lambda'_c}{\partial\bar{\mathrm{I}}_1}\\ &=\ddot{G}_{\text{iso}}\lambda'^2_c+\dot{G}_{\text{iso}}\lambda''_c. \end{aligned} \tag{A.3}$$

The derivative of isochoric cumulative density distribution G_{iso} with respect to actual chain stretch λ_c follows:

$$\dot{G}_{\text{iso}}\left(\lambda_c(\bar{\mathrm{I}}_1)\right)=\frac{a_0\,a_2}{\left(\lambda_c-1\right)}\exp\left(\frac{1}{4\,a_1}-\frac{\left(1+2\,a_1\ln\left(a_2(\lambda_c-1)\right)\right)^2}{4\,a_1}\right), \tag{A.4}$$

and the second order derivative of isochoric cumulative density distribution G_{iso} with respect to actual chain stretch λ_c is calculated as

$$\begin{aligned} \ddot{G}_{\text{iso}}\left(\lambda_c(\bar{\mathrm{I}}_1)\right)=\frac{a_0\,a_2}{\left(\lambda_c-1\right)^2}\exp\left(\frac{1}{4\,a_1}-\frac{\left(1+2\,a_1\ln\left(a_2(\lambda_c-1)\right)\right)^2}{4\,a_1}\right)\\ \left(2+2\,a_1\ln\left(a_2(\lambda_c-1)\right)\right). \end{aligned} \tag{A.5}$$

The first and second order derivative of current chain stretch $\lambda_c\left(\bar{\mathrm{I}}_1\right)$ concerning the first invariant of the isochoric Cauchy–Green deformation tensor $\bar{\mathrm{I}}_1$ are

$$\begin{aligned} \lambda'_c\left(\bar{\mathrm{I}}_1\right)&=\frac{1}{6}\left(\frac{\bar{\mathrm{I}}_1}{3}\right)^{-1/2}=\frac{1}{6}\lambda_c^{-1/2}\\ \lambda''_c\left(\bar{\mathrm{I}}_1\right)&=-\frac{1}{36}\left(\frac{\bar{\mathrm{I}}_1}{3}\right)^{-3/2}=\frac{1}{36}\lambda_c^{-3/2} \end{aligned} \tag{A.6}$$

The computation of the parameters a_0, a_1 and a_2 are given in Eq. (9). By combining Eq. (A.4), (A.5) and (A.6), the first and second order derivatives of free energy W_{iso} are evaluated to derive the stress and tangent tensors. The respective derivatives of the free energy function are

$$\begin{aligned} W'_{\text{iso}}&=G_{\text{iso}}\Psi'_{\text{iso}}+G'_{\text{iso}}\Psi_{\text{iso}}=G_{\text{iso}}\Psi'_{\text{iso}}+\dot{G}_{\text{iso}}\lambda'_c\Psi_{\text{iso}},\\ W''_{\text{iso}}&=G_{\text{iso}}\Psi''_{\text{iso}}+2G'_{\text{iso}}\Psi'_{\text{iso}}+G''_{\text{iso}}\Psi_{\text{iso}}\\ &=G_{\text{iso}}\Psi''_{\text{iso}}+2\dot{G}_{\text{iso}}\lambda'_c\Psi_{\text{iso}}+\left(\ddot{G}_{\text{iso}}\lambda'^2_c+\dot{G}_{\text{iso}}\lambda''_c\right)\Psi_{\text{iso}}. \end{aligned} \tag{A.7}$$

A.2. Volumetric part of free energy

Due to the nearly incompressible behaviour of the material, the volumetric part of free energy density is dependent on the volume ratio. With these considerations, the free energy function is based on the Jacobian J and the actual chain stretch

$$W_{\text{vol}}(J,\lambda_m)=\Psi_{\text{vol}}(J)\left(\int_1^{\infty} g_{\text{vol}}(\lambda_m)\mathrm{d}\lambda_m-\int_1^{\lambda_c} g_{\text{vol}}(\lambda_m)\mathrm{d}\lambda_m\right), \tag{A.8}$$

where the volumetric part of free energy is a simple quadratic function of Jacobian J [51]

$$\Psi_{\text{vol}}(J)=\frac{1}{E}(J-1)^2,\ \text{with}\ J=\sqrt{\bar{\mathrm{I}}_3}, \tag{A.9}$$

where E is the compression modulus. By substituting Eq. (A.9) in (A.8) leads to the volumetric part of the micromechanical free energy

$$\begin{aligned} W_{\text{vol}}(J,\lambda_m)&=\frac{1}{E}(J-1)^2\left(1-\int_1^{\lambda_c} g_{\text{vol}}(\lambda_m)\mathrm{d}\lambda_m\right)\\ &=\frac{1}{E}(J-1)^2(1-G_{\text{vol}}\left(\lambda_c(J)\right)). \end{aligned} \tag{A.10}$$

First-order derivative of volumetric cumulative density distribution function $G'_{\text{vol}}\left(\lambda_c(J)\right)$ is derived because of the implicit dependence on the Jacobian J

$$G'_{\text{vol}}\left(\lambda_c(J)\right)=\frac{\partial G_{\text{vol}}}{\partial\lambda_c}\frac{\partial\lambda_c}{\partial J}=\dot{G}_{\text{vol}}\lambda'_c\ \text{where}\ \lambda_c(J)=J^{1/3}. \tag{A.11}$$

The second order derivative of the volumetric form of cumulative density distribution function $G''_{\text{vol}}\left(\lambda_c(J)\right)$ can be derived by applying the chain rule

$$\begin{aligned} G''_{\text{vol}}\left(\lambda_c(J)\right)&=\frac{\partial}{\partial J}\left(\dot{G}_{\text{vol}}\lambda'_c\right)=\frac{\partial\dot{G}_{\text{vol}}}{\partial\lambda_c}\frac{\partial\lambda_c}{\partial J}\lambda'_c+\dot{G}_{\text{vol}}\frac{\partial\lambda'_c}{\partial J}\\ &=\ddot{G}_{\text{vol}}\lambda'^2_c+\dot{G}_{\text{vol}}\lambda''_c. \end{aligned} \tag{A.12}$$

$\dot{G}_{\text{vol}}\left(\lambda_c(J)\right)$ given in Eq. (A.11) is computed as the partial derivative of $G_{\text{vol}}\left(\lambda_c(J)\right)$ with current chain stretch $\lambda_c(J)$

$$\dot{G}_{\text{vol}}\left(\lambda_c(J)\right) = \frac{a_0 a_2}{\left(\lambda_c - 1\right)} \exp\left(\frac{1}{4\,a_1} - \frac{\left(1 + 2a_1 \ln\left(a_2(\lambda_c - 1)\right)\right)^2}{4\,a_1}\right), \tag{A.13}$$

and $\ddot{G}_{\text{vol}}\left(\lambda_c(J)\right)$ required in derivation of Eq. (A.12) is

$$\ddot{G}_{\text{vol}}\left(\lambda_c(J)\right) = \frac{a_0 a_2}{\left(\lambda_c - 1\right)^2} \exp\left(\frac{1}{4\,a_1} - \frac{\left(1 + 2a_1 \ln\left(a_2(\lambda_c - 1)\right)\right)^2}{4\,a_1}\right) \left(2 + 2a_1 \ln\left(a_2(\lambda_c - 1)\right)\right). \tag{A.14}$$

First and second order derivatives of the current chain stretch $\lambda_c(J)$ needed to derive Eq. (A.11) and (A.12) are

$$\begin{aligned} \lambda_c'(J) &= \frac{1}{3} J^{-1/3} = \frac{1}{3}\lambda_{\text{vol}}^{-1}, \\ \lambda_c''(J) &= -\frac{1}{9} J^{-4/3} = -\frac{1}{9}\lambda_{\text{vol}}^{-4}. \end{aligned} \tag{A.15}$$

To evaluate of stress and tangent tensors of the desired material model, one must derive first and second-order derivatives of the free energy function. The first- and second-order derivatives of the volumetric part of micromechanical free energy density W_{vol} are

$$\begin{aligned} W_{\text{vol}}' &= G_{\text{vol}}\Psi_{\text{vol}}' + G_{\text{vol}}'\Psi_{\text{vol}} = G_{\text{vol}}\Psi_{\text{vol}}' + \dot{G}_{\text{vol}}\lambda_c'\Psi_{\text{vol}} \\ W_{\text{vol}}'' &= G_{\text{vol}}\Psi_{\text{vol}}'' + 2G_{\text{vol}}'\Psi_{\text{vol}}' + G_{\text{vol}}''\Psi_{\text{vol}} \\ &= G_{\text{vol}}\Psi_{\text{vol}}'' + 2\dot{G}_{\text{vol}}\lambda_c'\Psi_{\text{vol}} + \left(\ddot{G}_{\text{vol}}\lambda_c'^2 + \dot{G}_{\text{vol}}\lambda_c''\right)\Psi_{\text{vol}}. \end{aligned} \tag{A.16}$$

Appendix B. Stress and elasticity tensors

The stress tensor in the updated Lagrangian formulation is obtained by applying a push-forward operation over the second Piola–Kirchhoff stress tensor. The stress tensor involved in the updated Lagrangian formulation is the Kirchhoff stress tensor $\boldsymbol{\tau}$ or the Cauchy stress tensor $\mathbf{T}$. In here, the Cauchy stress tensor $\mathbf{T}$ is calculated from the Kirchhoff stress tensor $\boldsymbol{\tau}$, where the Kirchhoff stresses $\boldsymbol{\tau}$ are

$$\begin{aligned} \boldsymbol{\tau}_{\text{eq}}\left(\bar{\mathbf{B}}, \lambda_m\right) &= 2\mathbf{B} \cdot \frac{\partial W_{\text{eq}}\left(\bar{\mathrm{I}}_1^{\bar{\mathbf{B}}}, \lambda_m\right)}{\partial \mathbf{B}} = 2J^{-2/3}\left(W_{\text{eq}}\right)'\left(\bar{\mathbf{B}} - \frac{1}{3}\bar{\mathrm{I}}_1^{\bar{\mathbf{B}}}\mathbf{I}\right); \\ \boldsymbol{\tau}_{\text{vol}}\left(J, \lambda_m\right) &= 2\mathbf{B} \cdot \frac{\partial W_{\text{vol}}\left(J, \lambda_m\right)}{\partial \mathbf{B}} = J W_{\text{vol}}\mathbf{I}; \\ \boldsymbol{\tau}_{\text{neq}}^{j}\left(\bar{\mathbf{B}}_e^{j}, \lambda_m\right) &= 2\bar{\mathbf{B}}_e^{j} \cdot \frac{\partial W_{\text{neq}}^{j}\left(\bar{\mathrm{I}}_1^{\bar{\mathbf{B}}_e^{j}}, \lambda_m\right)}{\partial \bar{\mathbf{B}}_e^{j}} = 2J^{-2/3}\left(W_{\text{neq}}^{j}\right)'\left(\bar{\mathbf{B}}_e^{j} - \frac{1}{3}\bar{\mathrm{I}}_1^{\bar{\mathbf{B}}_e^{j}}\mathbf{I}\right). \end{aligned} \tag{B.1}$$

and the Cauchy stresses are calculated

$$\mathbf{T} = J^{-1}\boldsymbol{\tau}. \tag{B.2}$$

In non-linear finite element simulation the solution is often solved incrementally using Newton's method and computation of the tangent is crucial for the solution. The tangent tensor of the softening micromechanical free energy is

$$\begin{aligned} \overset{4}{\boldsymbol{\kappa}} &= 4\mathbf{B} \cdot \frac{\partial^2 W\left(\bar{\mathrm{I}}_1^{\bar{\mathbf{B}}}, \bar{\mathrm{I}}_1^{\bar{\mathbf{B}}_e^{j}}, J, m\right)}{\partial \mathbf{B}\,\partial \mathbf{B}} \cdot \mathbf{B} = \overset{4}{\boldsymbol{\kappa}}_{\text{eq}} + \overset{4}{\boldsymbol{\kappa}}_{\text{vol}} + \overset{4}{\boldsymbol{\kappa}}_{\text{neq}}, \\ \overset{4}{\boldsymbol{\kappa}}_{\text{eq}} &= 4\mathbf{B} \cdot \frac{\partial^2 W_{\text{eq}}\left(\bar{\mathrm{I}}_1^{\bar{\mathbf{B}}}, m\right)}{\partial \mathbf{B}\,\partial \mathbf{B}} \cdot \mathbf{B}; \quad \overset{4}{\boldsymbol{\kappa}}_{\text{vol}} = 4\mathbf{B} \cdot \frac{\partial^2 W_{\text{vol}}\left(J, m\right)}{\partial \mathbf{B}\,\partial \mathbf{B}} \cdot \mathbf{B}, \\ \overset{4}{\boldsymbol{\kappa}}_{\text{neq}} &= 4\bar{\mathbf{B}}_e^{j} \cdot \frac{\partial^2 W_{\text{neq}}^{j}\left(\bar{\mathrm{I}}_1^{\bar{\mathbf{B}}_e^{j}}, m\right)}{\partial \bar{\mathbf{B}}_e^{j}\,\partial \bar{\mathbf{B}}_e^{j}} \cdot \bar{\mathbf{B}}_e^{j}. \end{aligned} \tag{B.3}$$

The individual components of the spatial elasticity tensor take the form

$$\begin{aligned} \overset{4}{\boldsymbol{\kappa}}_{\text{eq}} &= 4\left(W_{\text{eq}}\left(\bar{\mathrm{I}}_1^{\bar{\mathbf{B}}}, m\right)\right)'\left(\mathbf{I} \otimes \bar{\mathbf{B}}\right)^{s_{24}} + 4\left(W_{\text{eq}}\left(\bar{\mathrm{I}}_1^{\bar{\mathbf{B}}}, m\right)\right)''\left(\bar{\mathbf{B}} \otimes \bar{\mathbf{B}}\right) - \\ &\quad \frac{4}{3}\left(\bar{\mathrm{I}}_1^{\bar{\mathbf{B}}}\left(W_{\text{eq}}\left(\bar{\mathrm{I}}_1^{\bar{\mathbf{B}}}, m\right)\right)'' + \left(W_{\text{eq}}\left(\bar{\mathrm{I}}_1^{\bar{\mathbf{B}}}, m\right)\right)'\right)\left(\bar{\mathbf{B}} \otimes \mathbf{I} + \mathbf{I} \otimes \bar{\mathbf{B}}\right) + \\ &\quad \frac{4}{9}\left(\left(\bar{\mathrm{I}}_1^{\bar{\mathbf{B}}}\right)^2\left(W_{\text{eq}}\left(\bar{\mathrm{I}}_1^{\bar{\mathbf{B}}}, m\right)\right)'' + \bar{\mathrm{I}}_1^{\bar{\mathbf{B}}}\left(W_{\text{eq}}\left(\bar{\mathrm{I}}_1^{\bar{\mathbf{B}}}, m\right)\right)'\right)\left(\mathbf{I} \otimes \mathbf{I}\right) \\ \overset{4}{\boldsymbol{\kappa}}_{\text{vol}} &= \left(J^2\left(W_{\text{vol}}\left(J, m\right)\right)'' + J\left(W_{\text{vol}}\left(J, m\right)\right)'\right)\mathbf{I} \otimes \mathbf{I} \\ \overset{4}{\boldsymbol{\kappa}}_{\text{neq}} &= 4W_{\text{neq}}'\left(\bar{\mathrm{I}}_1^{\bar{\mathbf{B}}_e^{j}}, m\right)\left(\mathbf{I} \otimes \bar{\mathbf{B}}\right)^{s_{24}} + 4W_{\text{neq}}''\left(\bar{\mathrm{I}}_1^{\bar{\mathbf{B}}_e^{j}}, m\right)\left(\bar{\mathbf{B}} \otimes \bar{\mathbf{B}}\right) - \\ &\quad \frac{4}{3}\left(\bar{\mathrm{I}}_1^{\bar{\mathbf{B}}_e^{j}} W_{\text{neq}}''\left(\bar{\mathrm{I}}_1^{\bar{\mathbf{B}}_e^{j}}, m\right) + W_{\text{neq}}'\left(\bar{\mathrm{I}}_1^{\bar{\mathbf{B}}_e^{j}}, m\right)\right)\left(\bar{\mathbf{B}} \otimes \mathbf{I} + \mathbf{I} \otimes \bar{\mathbf{B}}\right) + \\ &\quad \frac{4}{9}\left(\left(\bar{\mathrm{I}}_1^{\bar{\mathbf{B}}_e^{j}}\right)^2 W_{\text{neq}}''\left(\bar{\mathrm{I}}_1^{\bar{\mathbf{B}}_e^{j}}, m\right) + \bar{\mathrm{I}}_1^{\bar{\mathbf{B}}_e^{j}} W_{\text{neq}}'\left(\bar{\mathrm{I}}_1^{\bar{\mathbf{B}}_e^{j}}, m\right)\right)\left(\mathbf{I} \otimes \mathbf{I}\right). \end{aligned} \tag{B.4}$$

In the definition of the isochoric component of the equilibrium W_{eq} and non-equilibrium W_{neq}^{j} of jth Maxwell element free energy functions are motivated by the Neo-Hook energy function for its simplicity which is required to implement the viscoelastic material model based on micromechanical material model. Based on the fundamental idea discussed in the development of the viscoelastic material model, the micromechanical free energy functions take the form

$$\begin{aligned} &\Psi_{\text{eq}}\left(\bar{\mathrm{I}}_1^{\bar{\mathbf{B}}}\right) = c_{10}\left(\bar{\mathrm{I}}_1^{\bar{\mathbf{B}}} - 3\right) \text{results in } W_{\text{eq}} = \Psi_{\text{eq}}\left(\bar{\mathrm{I}}_1^{\bar{\mathbf{B}}}\right) G\left(\lambda_c\left(\bar{\mathrm{I}}_1^{\bar{\mathbf{B}}}\right)\right), \\ &\Psi_{\text{neq}}^{j}\left(\bar{\mathrm{I}}_1^{\bar{\mathbf{B}}_e^{j}}\right) = c_{10j}\left(\bar{\mathrm{I}}_1^{\bar{\mathbf{B}}_e^{j}} - 3\right) \text{results in } W_{\text{neq}}^{j} = \Psi_{\text{eq}}\left(\bar{\mathrm{I}}_1^{\bar{\mathbf{B}}_e^{j}}\right) G\left(\lambda_c\left(\bar{\mathrm{I}}_1^{\bar{\mathbf{B}}_e^{j}}\right)\right), \end{aligned} \tag{B.5}$$

and the free energy for the volumetric component of the equilibrium part is introduced with a quadratic function of Jacobian as follows

$$\Psi_{\text{vol}}(J) = \frac{1}{E}(J-1)^2 \text{ results in } W_{\text{vol}} = \Psi_{\text{vol}}(J)\, G\left(\lambda_c(J)\right), \tag{B.6}$$

where D corresponds to the shear modulus. When $J = 1$ the material corresponds to the incompressible material. The first and second-order derivatives of the volumetric free energy are given in Eq. (A.16)

Appendix C. Modelling transport of moisture

The diffusion of moisture in the crosslinked polyurethane adhesive is modelled here with the Langmuir-type diffusion model [22], so that the dispersion of moisture concentration into mobile and immobile moisture concentrations are taken into consideration. The Langmuir-type diffusion model is formulated as follows:

$$\dot{m} = D\,\Delta m_f = D\,\text{div}\left(\text{grad}\left(m - m_b\right)\right), \tag{C.1}$$

where D is diffusion coefficient, m_f is the mobile moisture concentration, m_b is immobile moisture concentration and $m = m_f + m_b$ is total moisture concentration. The moisture distribution along the material is characterised by $m = 0$ for the dry state and $m = m^{\text{eq}}$ for the equilibrium state. The diffusion Eq. (C.1) is supplemented by an evolution equation to compute immobile moisture concentration m_b

$$\dot{m}_b = \alpha m_f - \beta m_b. \tag{C.2}$$

The simple idea behind the evolution equation is that moisture is bound faster when there is a large amount of mobile moisture. In contrast, when the bound moisture concentration is large, a significant amount of mobile moisture is released to become mobile. The two constants α and β describe the time constants of these two effects. An equilibrium moisture distribution occurs when the time derivative of the immobile moisture concentration of the evolution equation becomes zero. As a result, the evolution equation leads to

$$\alpha m_f^{\text{eq}} = \beta m_b^{\text{eq}}. \tag{C.3}$$

The mobile and immobile concentration at the equilibrium condition is evaluated by substituting total moisture concentration in Eq. (C.3). The resulting mobile and immobile moisture concentrations are

$$m_f^{\mathrm{eq}} = \frac{m^{\mathrm{eq}}}{1+\alpha/\beta}, \qquad m_b^{\mathrm{eq}} = \frac{m^{\mathrm{eq}}\alpha/\beta}{1+\alpha/\beta}. \tag{C.4}$$

Both boundary and initial conditions are needed to solve the Langmuir model. The initial conditions are defined for the entire material volume Ω at the time $t_0 = 0$ given

$$m(\mathbf{x}, t=0) = m(\mathbf{x}), \quad m_b(\mathbf{x}, t=0) = m_{b_0}(\mathbf{x}), \tag{C.5}$$

where the spatial functions of the total moisture concentration $m(\mathbf{x})$ and the bound moisture concentration $m_{b_0}(\mathbf{x})$ are used to define the initial condition of moisture distribution. The boundary conditions are discretised into Dirichlet and Neumann conditions. On the Dirichlet boundaries, $\partial\Omega_m^D$ is defined with the concentration values as the Dirichlet boundary condition. In contrast, the Neumann boundary $\partial\Omega_{\mathbf{q}}^N$ is applied with the moisture flux. The boundary surfaces need to satisfy the condition

$$\partial\Omega_m^D \cup \partial\Omega_{\mathbf{q}}^N = \partial\Omega, \qquad \partial\Omega_m^D \cap \partial\Omega_{\mathbf{q}}^N = \varnothing \tag{C.6}$$

over the entire material volume Ω. The Dirichlet boundaries are applied with the moisture concentration as follows

$$m(m(\mathbf{x}, t)) = m^{\mathrm{eq}} \ \forall \ \mathbf{x} \in \partial\Omega_m^D \tag{C.7}$$

and the moisture flux is applied on the Neumann boundaries, and the Neumann boundary condition is given as:

$$\mathbf{q}\cdot\mathbf{n} = D\mathrm{grad}m_f \cdot \mathbf{n} = \mathbf{q}(\mathbf{x}, t) \ \forall \ \mathbf{x} \in \partial\Omega_{\mathbf{q}}^N. \tag{C.8}$$

As a result, the moisture flux takes the form

$$\mathbf{q} = D\frac{\partial m_f}{\partial \mathbf{x}} = D\mathrm{grad}\, m_f \tag{C.9}$$

where $\mathbf{n}$ is the normal outward vector on the boundary.

Data availability

Data will be made available on request.

References

[1] A. Mubashar, I.A. Ashcroft, G.W. Critchlow, A.D. Crocombe, Moisture absorption-desorption effects in adhesive joints, Int. J. Adhes. Adhes. 29 (2009) 751–760, http://dx.doi.org/10.1016/j.ijadhadh.2009.05.001.

[2] M. Mooney, A theory of large elastic deformation, J. Appl. Phys. 11 (1940) 582–592, http://dx.doi.org/10.1063/1.1712836.

[3] R.S. Rivlin, Large elastic deformations of isotropic materials IV. Further developments of the general theory, Philos. Trans. R. Soc. Lond. Ser. A Math. Phys. Eng. Sci. 241 (1948) 379–397, http://dx.doi.org/10.1098/rsta.1948.0024.

[4] O.H. Yeoh, Some forms of the strain energy function for rubber, Rubber Chem. Technol. 66 (1993) 754–771, http://dx.doi.org/10.5254/1.3538343.

[5] W. Ogden Raymond, Non-Linear Elastic Deformations, Dover, 1997.

[6] H.M. James, E. Guth, Theory of the elastic properties of rubber, J. Chem. Phys. 11 (10) (1943) 455–481, http://dx.doi.org/10.1063/1.1723785.

[7] A.G. James, A. Green, G.M. Simpson, Strain energy functions of rubber. I. Characterization of gum vulcanizates, Appl. Polym. Sci. 19 (1975) 2033–2058, http://dx.doi.org/10.1002/app.1975.070190723.

[8] M.E. Arruda, M.C. Boyce, A three-dimensional constitutive model for the large stretch behavior of rubber elastic materials, J. Mech. Phys. Solids 41 (1993) 389–412, http://dx.doi.org/10.1016/0022-5096(93)90013-6.

[9] C. Miehe, S. Göktepe, F. Lulei, A micro-macro approach to rubber-like materials-part I: the non-affine micro-sphere model of rubber elasticity, J. Mech. Phys. Solids 52 (2004) 2617–2660, http://dx.doi.org/10.1016/j.jmps.2004.03.011.

[10] F. Bueche, Molecular basis for the mullins effect, J. Appl. Polym. Sci. 4 (1960) 107–114, http://dx.doi.org/10.1002/app.1960.070041017.

[11] J.A.C. Harwood, L. Mullins, A.R. Payne, Stress softening in natural rubber vulcanizates. Part II. Stress softening effects in pure gum and filler loaded rubbers, J. Appl. Polym. Sci. 9 (1965) 3011–3021, http://dx.doi.org/10.1002/app.1965.070090907.

[12] L.R.G. Treloar, The photoelastic properties of short-chain molecular networks, Trans. Faraday Soc. 50 (1954) 881–896, http://dx.doi.org/10.1039/TF9545000881.

[13] W. Kuhn, F. Grün, Beziehungen zwischen elastischen konstanten und dehnungsdoppelbrechung hochelastischer stoffe, Kolloid-Z. 101 (1942) 248–271, http://dx.doi.org/10.1007/BF01793684.

[14] S. Govindjee, J. Simo, A micro-mechanically based continuum damage model for carbon black-filled rubbers incorporating Mullins effect, J. Mech. Phys. Solids 39 (1991) 87–112, http://dx.doi.org/10.1016/0022-5096(91)90032-J.

[15] Stephen B. Smeulders, S. Govindjee, A phenomenological model of an elastomer with an evolving molecular weight distribution, J. Rheol. 43 (1999) 393–414, http://dx.doi.org/10.1122/1.551042.

[16] G. Marckmann, E. Verron, L. Gornet, G. Chagnon, P. Charrier, P. Fort, A theory of network alteration for the Mullins effect, J. Mech. Phys. Solids 50 (2002) 2011–2028, http://dx.doi.org/10.1016/S0022-5096(01)00136-3.

[17] S. Göktepe, C. Miehe, A micro–macro approach to rubber-like materials. Part III: The micro-sphere model of anisotropic mullins-type damage, J. Mech. Phys. Solids 53 (2005) 2259–2283, http://dx.doi.org/10.1016/j.jmps.2005.04.010.

[18] P. Bažant, B.H. Oh, Efficient numerical integration on the surface of a sphere, ZAMM - J. Appl. Math. Mech. 66 (1986) 37–49, http://dx.doi.org/10.1002/zamm.19860660108.

[19] R. Dargazany, M. Itskov, A network evolution model for the anisotropic mullins effect in carbon black filled rubbers, Int. J. Solids Struct. 46 (2009) 2967–2977, http://dx.doi.org/10.1016/j.ijsolstr.2009.03.022.

[20] M. Itskov, A. Knyazeva, A rubber elasticity and softening model based on chain length statistics, Int. J. Solids Struct. 80 (2016) 512–519, http://dx.doi.org/10.1016/j.ijsolstr.2015.10.011.

[21] J.E. Huacuja-Sánchez, K. Müller, W. Possart, Water diffusion in a crosslinked polyether-based polyurethane adhesive, Int. J. Adhes. Adhes. 66 (2016) 167–175, http://dx.doi.org/10.1016/j.ijadhadh.2016.01.005.

[22] H.G. Carter, K.G. Kibler, Langmuir-type model for anomalous moisture diffusion in composite resins, J. Compos. Mater. 12 (1978) 118–131, http://dx.doi.org/10.1177/002199837801200201.

[23] S. Popineau, C. Rondeau-Mouro, C. Sulpice-Gaillet, E.R.M. Shanahan, Free/bound water absorption in an epoxy adhesive, Polymer 46 (2005) 10733–10740, http://dx.doi.org/10.1016/j.polymer.2005.09.008.

[24] A. Ameli, N.V. Datla, M. Papini, J.K. Spelt, Hygrothermal properties of highly toughened epoxy adhesives, J. Adhes. 86 (2010) 698–725, http://dx.doi.org/10.1080/00218464.2010.482405.

[25] S. Roy, J.N. Reddy, Finite-element models of viscoelasticity and diffusion in adhesively bonded joints, Internat. J. Numer. Methods Engrg. 26 (1988) 2531–2546, http://dx.doi.org/10.1002/nme.1620261111, John Wiley & Sons Ltd.

[26] W. Hong, X. Zhao, J. Zhou, Z. Suo, A theory of coupled diffusion and large deformation in polymeric gels, J. Mech. Phys. Solids 56 (2008) 1779–1793, http://dx.doi.org/10.1016/j.jmps.2007.11.010.

[27] S.A. Chester, C. Leo, L. Anand, A finite element implementation of a coupled diffusion-deformation theory for elastomeric gels, Int. J. Solids Struct. 52 (2015) 1–18, http://dx.doi.org/10.1016/j.ijsolstr.2014.08.015.

[28] M. Haghighi-Yazdi, P. Lee-Sullivan, Modeling of structural mechanics, moisture diffusion, and heat conduction coupled with physical aging in thin plastic plates, Acta Mech. 225 (2014) 29–950, http://dx.doi.org/10.1007/s00707-013-1007-y.

[29] H. Su, H. Yan, B. Jin, Finite element method for coupled diffusion-deformation theory in polymeric gel based on slip-link model, Appl. Math. Mech.-Engl. Ed. 39 (2018) 581–596, http://dx.doi.org/10.1007/s10483-018-2315-7.

[30] F. Goldschmidt, S. Diebels, Modelling and numerical investigations of the mechanical behavior of polyurethane under the influence of moisture, Arch. Appl. Mech. 85 (2015) 1035–1042, http://dx.doi.org/10.1007/s00419-014-0943-x.

[31] P. Sharma, A. Sambale, M. Stommel, M. Maisl, H.-G. Herrmann, S. Diebels, Moisture transport in PA6 and its influence on the mechanical properties, Contin. Mech. Thermodyn. 32 (2020) 307–325, http://dx.doi.org/10.1007/s00161-019-00815-w.

[32] W. Kuhn, Beziehungen zwischen molekülgröße, statistischer molekülgestalt und elastischen eigenschaften hochpolymerer stoffe, Kolloid-Z. 76 (1936) 258–271, http://dx.doi.org/10.1007/BF01451143.

[33] H.V. Wesslau, Die molekulargewichtsverteilung einiger niederdruckpolyäthylene, Macromol. Chem. Phys. 20 (1956) 111–142, http://dx.doi.org/10.1002/macp.1956.020200109.

[34] G. Marckmann, E. Verron, Comparison of hyperelastic models for rubber-like materials, Rubber Chem. Technol. 79 (5) (2006) 835–858, http://dx.doi.org/10.5254/1.3547969.

[35] C. Miehe, Aspects of the formulation and finite element implementation of large strain isotropic elasticity, Internat. J. Numer. Methods Engrg. 37 (12) (1994) 1981–2004, http://dx.doi.org/10.1002/nme.1620371202.

[36] P. Haupt, A. Lion, On finite linear viscoelasticity of incompressible isotropic materials, Acta Mech. 159 (2002) 87–124, http://dx.doi.org/10.1007/BF01171450.

[37] E.H. Lee, Elastic-plastic deformation at finite strains, ASME. J. Appl. Mech. 36 (1969) 1–6, http://dx.doi.org/10.1115/1.3564580.

[38] P.J. Flory, Theory of elasticity of polymer networks. The effect of local constraints on junctions, J. Chem. Phys. 66 (1977) 5720–5729, http://dx.doi.org/10.1063/1.433846.

[39] S. Hartmann, Computation in finite-strain viscoelasticity: finite elements based on the interpretation as differential–algebraic equations, Comput. Methods Appl. Mech. Engrg. 191 (2002) 1439–1470, http://dx.doi.org/10.1016/S0045-7825(01)00332-2.

[40] J.C. Simo, On a fully three-dimensional finite-strain viscoelastic damage model: Formulation and computational aspects, Comput. Methods Appl. Mech. Engrg. 60 (1987) 153–173, http://dx.doi.org/10.1016/0045-7825(87)90107-1.

[41] B.D. Coleman, W. Noll, The thermodynamics of elastic materials with heat conduction and viscosity, Arch. Ration. Mech. Anal. 13 (1963) 167–178, http://dx.doi.org/10.1007/BF01262690.

[42] A. Lion, Thermomechanik Von Elastomeren, Vol. 12, Berichte des Institut für Mechanik (Bericht 1/2000), Universität Gesamthochschule Kassel, 2000.

[43] K. Seldan, Viskoelastisches Materialverhalten von Elastomerwerkstoffen: Experimentelle Untersuchung und Modellbildung, (Dissertation), Berichte des Institut für Mechanik (Bericht 2/2001), Universität Gesamthochschule Kassel, 2000.

[44] P. Haupt, Continuum Mechanics and Theory of Materials second ed., Springer-Verlag Berlin, Heidelberg, 2002, http://dx.doi.org/10.1007/978-3-662-04775-0.

[45] D. Arndt, W. Bangerth, et al., The deal.ii library, version 8.5, J. Numer. Math. 25 (2017) 137–145, http://dx.doi.org/10.1515/jnma-2017-0058.

[46] W. Bangerth, R. Hartmann, G. Kanschat, Deal.II-A general-purpose object-oriented finite element library, ACM Trans. Math. Software 33 (2007) http://dx.doi.org/10.1145/1268776.1268779.

[47] Y. Saad, M.H. Schultz, A generalized minimal residual algorithm for solving nonsymmetric linear systems, SIAM J. Sci. Stat. Comput. 7 (1986) 856–869, http://dx.doi.org/10.1137/0907058.

[48] J. Crank, P. Nicolson, A practical method for numerical evaluation of solutions of partial differential equations of the heat-conduction type, Adv. Comput. Math. 6 (1996) 207–226, http://dx.doi.org/10.1007/BF02127704.

[49] S. Mazumder, Chapter 5 - treatment of the time derivative (parabolic and hyperbolic PDEs), in: Numerical Methods for Partial Differential Equations Academic Press, 2019, pp. 219–275, http://dx.doi.org/10.1016/B978-0-12-849894-1.00005-6.

[50] J.A. Nelder, R. Mead, A simplex method for function minimization, Comput. J. 7 (1965) 308–313, http://dx.doi.org/10.1093/comjnl/7.4.308.

[51] G.A. Holzapfel, Nonlinear Solid Mechanics: A Continuum Approach for Engineering Wiley, 2000.